This is a preprint of an article published in ***MRS Communications***, Volume 14, pages 1313-1318 (2024).
The final authenticated version is available online at: https://doi.org/10.1557/s43579-024-00634-4

The Creation of Defects in Cu-Doped TiO_2 Memristive Devices

Bin Gu[a], Bo Zhang[a], Tomas Wagner[b,c*]*

[a]College of Physics, Hebei Normal University, Shijiazhuang 050024, China

[b]Center of Materials and Nanotechnologies, Faculty of Chemical Technology, University of Pardubice, nam. Cs. Legii 565, Pardubice 530 02, Czech Republic

[c]Department of General and Inorganic Chemistry, Faculty of Chemical Technology, University of Pardubice, Studentska 573, 532 10 Pardubice, Czech Republic

Abstract Memristors are promising for use as nonvolatile memory and artificial synaptic devices. However, the industrial application of memristors has been restricted by the occurrence of fatigue, the mechanism of which is still under debate. In this paper, we systematically investigated the mechanism of defect generation created by Joule heating in Cu-doped TiO_2 memristive device. The results also demonstrated that the Joule heat for artificial synaptic emulation was less severe than that for digital data storage.

Keywords: Physical vapor deposition, Semiconductors, Thin films

Introduction

Two-terminal memristors have emerged as promising devices for overcoming the von Neumann bottomneck. Memristors can mimic the biological brain through the fusion of storage and computation[1]. Memristive devices with gradual or analogous SET and RESET can be utilized for emulating biosynapse behavior, whereas those with abrupt SET and RESET are suitable only for digital memory storage applications [2]- [3]. However, the fatigue of memristive devices is a barrier to their industrialization, the reason still needs to be explored.

Metal-doped TiO_2 is commonly utilized for resistive switching and synaptic emulation[4,5]. Yang et al. reported a phenomenon of defect creation during the electroforming process in a TiO_2-based memristive device, which was explained via the generation of O_2 gas[6]. Kolar et al. observed the depletion of metallic electrodes in Ag-doped AsS_2 electrolyte films after successive DC sweeps[7]. Furthermore, Joule heating also influenced the performance of memristive devices and caused their failure. In our previous papers, we investigated the surface morphology of W/Cu-doped SiO_2/Cu memristive devices after DC sweeps, and the results suggested that the Joule heat was closely related to the generation of defects. Different types of defects, including pores, dendrites and particles, were reported in these papers [8,9].

In this paper, we investigated the defects of memristive devices based on Cu-doped TiO_2. The I-V curve was measured for digital data storage and synaptic emulation. After the SET operation, defects in the memristive device, including particles and pores, were present in the region of the electrode. Although the compliance current protected the device from overshooting, further experiments suggested that Joule heating led to the formation of defects. However, because a low operating current was needed, defects were not created in the memristive devices for biosynapse emulation. The present work could promote the development of memristive devices with stable working performance.

Experiment details

The devices were fabricated on a silica glass substrate with 3 layers (Cu/Cu-doped TiO_2/Al). The topmost Al electrodes were deposited via a stencil in a crossbar configuration, the size of which was 100 μm × 100 μm. All coating processes were conducted in a vacuum chamber at a base pressure of $1x10^{-5}$ mbar using argon gas (99.999%) at a flow rate of 30 sccm. First, inert Al electrode was deposited onto silica substrate by RF sputtering. Afterward, Cu-doped TiO_2 was deposited via cosputtering of a Cu target (DC 20 W, 10 mins) and a TiO_2 target (RF 50 W, 10 mins) with a thickness of 30nm. The active electrode Cu electrode was deposited onto Cu-doped TiO_2 via DC sputtering. I-V curves were measured via a Keithley 2600 multimeter equipped with tungsten probes, where the positive electrode contacted the underlying Cu electrode and the negative electrode contacted the topmost Al electrode. The DC sweep was measured from 2 V to -1 V with a step of 100 mV. The pulse measurement of analog modulation of conductance was also measured via a Keithley 2600 multimeter equipped with tungsten probes, which the length of pulses was calibrated via an oscilloscope (LOTO, OSC482). The potentiation and depression of conductance were modulated with positive (amplitude: 2.5 V, width: 100 ms)/negative spikes (amplitude: -1.8 V, width: 100 ms). All the samples were studied via scanning electron microscope imaging (SEM, Hitachi S4800) at 10 kV. Energy dispersive x-Ray spectroscopy (EDS) elemental maps for memristive devices were captured using Hitachi S4800 SEM equipped with **I**NCA Energy 350 EDS detector operated at 20 kV.

The composition of solid electrolyte layer (Cu doped TiO_2) was measured via X-ray photoelectron spectroscopy (XPS) using a ESCALAB QXi equipped with a monochromatic Al Kα X-ray source (1486.6 eV) operated at 150 W. The samples were analyzed under vacuum ($P < 10^{-8}$ mbar) with a pass energy of 100 eV (survey scans) or 20 eV (high-resolution scans). All the XPS peaks were calibrated for adventitious carbon with a C1s peak binding energy of 284.8 eV.

Results and discussion

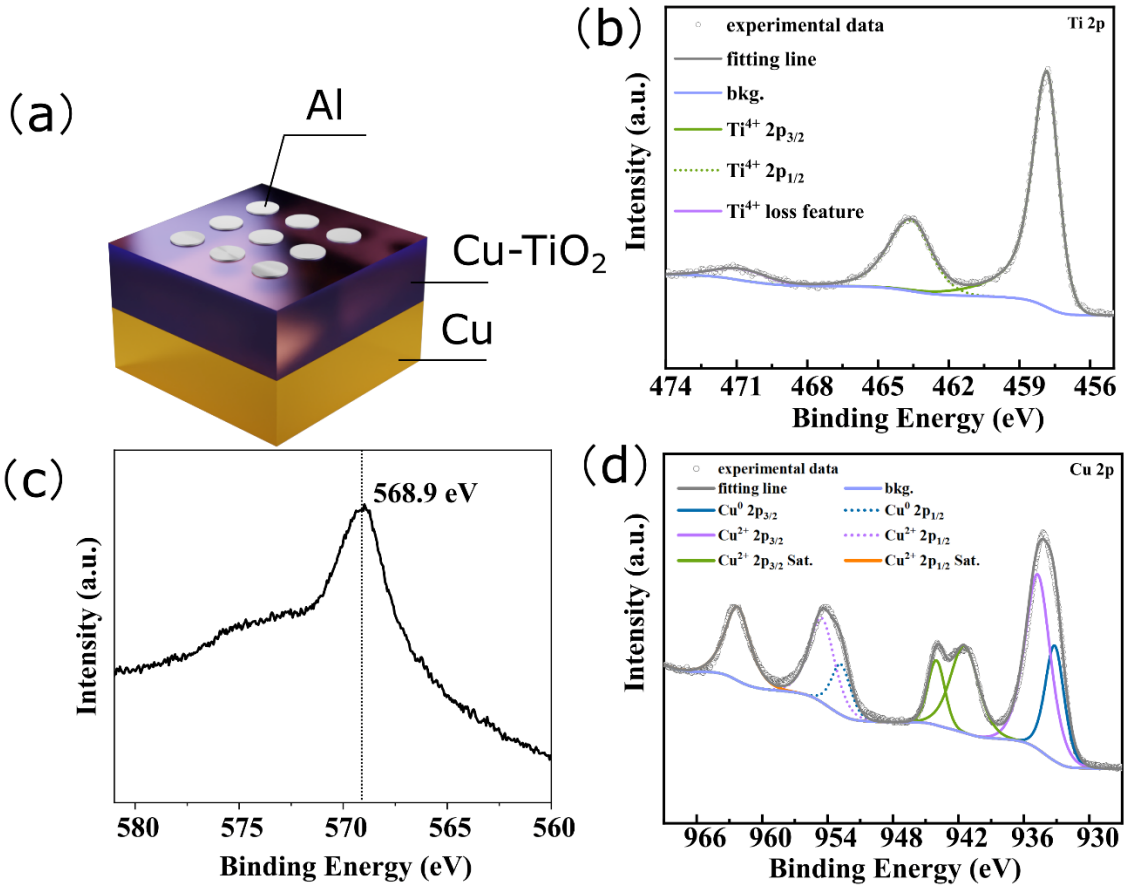

Figure 1 (a) Schematic illustration of the memristive cell; (b) high-resolution XPS spectrum of the Ti 2p region; (c) high-resolution XPS spectrum of the Cu $L_3M_{4,5}M_{4,5}$ region; (d) high-resolution XPS spectrum of the Cu 2p region.

A memristive cell was fabricated from the structure of Cu (bottom)/Cu-doped TiO_2/Al (top), where the Al top electrode was deposited via a stencil mask (Figure 1 (a)). The Cu-doped TiO_2 electrolyte layer was deposited by cosputtering from the ceramic TiO_2 target and copper target in an argon air environment. The elemental composition ($Cu_{85}(TiO_2)_{15}$) of the Cu-doped TiO_2 electrolyte layer was analyzed from XPS spectrum. The full spectrum is presented in Figure S1. In the spectrum of the Ti 2p region (Figure 1 (b)), the doublet peaks at $Ti2p_{3/2}$ (458.6 eV) and $Ti2p_{1/2}$ (464.4 eV) were attributed to spin-orbital splitting [10]. The shoulder $Ti2p_{1/2}$ peak at a binding energy of 460.2 eV represents the existence of Ti^{3+}. Since TiO_2 was doped with Cu, the valence state of Cu was also analyzed, as shown in Figure 1 (c) and (d), where the binding energy of the Auger peak (568.9 eV) in Figure 1(c) corresponds to the Cu^{2+} oxidation state[11]. As shown in Figure 1(d), two oxidation

states of Cu (Cu^0 and Cu^{2+}) were identified from the $2p_{3/2}$ peak. The precipitation of metallic element facilitates the analogue modulation of resistance in memristve device[3].

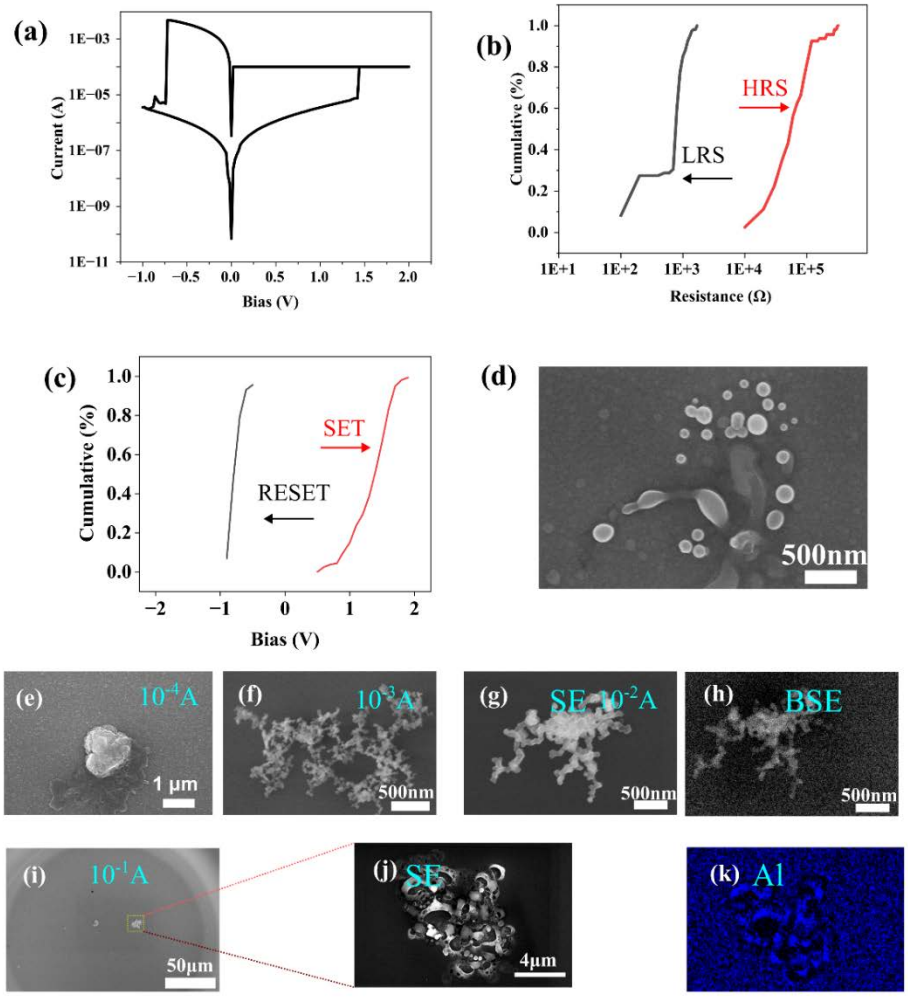

Figure 2 (a) I-V curve of the Cu/Cu-doped TiO_2/Al memristive device; (b) cumulative probability of the resistances for 160 cycles in the Cu/Cu-doped TiO_2/Al memristive device; (c) cumulative probability of the SET and RESET thresholds for 160 cycles in the Cu/Cu-doped TiO_2/Al memristive device; (d) SEM image of surface morphology after 160 successive cycles of DC sweep; (e) SEM image of the surface of the electrode after a positive DC sweep with a compliance current of 10^{-4}A; (f) SEM image of defects on the surface of the electrode after a positive DC sweep with a compliance current of 10^{-3}A; (g)-(h) SEM image of defects on the surface of the electrode after a positive DC sweep with a compliance current of 10^{-2}A (SE(g), BSE(h)); (i) SEM image of defects on the surface of the electrode after a positive DC sweep with a compliance current of 0.1A; (j) SEM images of pore defects enlarged from (i); (k) EDS mapping of the Al in (j).

To study the resistive switching of the memristor cell, I-V characteristics were measured using a Keithley 2600 instrument equipped with tungsten probes, in which the topmost Al electrode was in contact with the negative probe and the bottom Cu electrode was in contact with the positive electrode. The DC sweep was measured from 2 V to -1 V with a compliance current of 10^{-4} A for 160 successive cycles, and the first cycle is shown in Figure 2(a). This mechanism can be explained by the electrochemical metallization model. First, Cu ions migrated toward the topmost inert Al electrode. Afterward, the Cu was reduced as a conductive filament connected to the topmost and bottom electrodes. At this moment, referred to as the SET process, the current ramps up and switches the device from HRS (High Resistance State) to LRS (Low Resistance state). A reversed process occurred in a RESET process, which the conductive filament was dissolved with the help of Joule heating and current ramps down. At this moment, the resistance switched from the LRS to the HRS. The cumulative probability of the resistances is presented with an R_{off} and R_{on} ratio of 10, as shown in Figure 2 (b). The cumulative probability of SET/RESET thresholds is presented in Figure 2 (c). One can see stochastic fluctuations in the resistances and SET/RESET thresholds, which were partially caused by changes in the surface morphology. After 160 cycles, the bubble morphologies were observed via SEM, as shown in Figure 2 (d). In our opinion, such defects were mainly caused by Joule heating, which is directly related to the current flowing through the device. As discussed in our previous paper, a morphology similar to that of "bubbles" was observed. Due to the Joule heat produced by current, the body of the conductive filaments was vaporized. Therefore, the Cu-doped TiO_2 electrolyte layer detached from the substrate. Although the compliance current was utilized during the I-V measurement, defects of the pores and particles still appeared when the current increased to the compliance current in the SET process. Likewise, the surface morphology strongly depended on the sum of the current in the Cu/Cu-doped TiO_2/Al memristive device. Therefore, we measured the I-V curves of the sample from 0 V to the SET threshold with different compliance currents and checked the surface morphology after the I-V curve. The curve is presented in Figure S2. An SEM image of the sample surface is presented in Figure 2 (e)-(k). First, with a compliance current of 10^{-4} A, microsized particles were found at the center of the topmost electrode, suggesting the precipitation of Cu agglomerations, as shown in Figure 2 (e). The dendritic defect in Figure 2 (f) appeared in the device measured with a compliance current of 10^{-3}A. Similarly, dendritic defects can also be found in the measurement with a compliance current of 10^{-2} A. As shown in Figure 2(g) and (h), the SEM images in SE and BSE confirm that the defects consist of heavier elements, possibly Cu (Figure 2(e)). As shown in Figure 2 (i)-(k), the defects of the device that switched under a compliance current of 0.1 A presented a porous morphology, and further EDS mapping of the aluminum revealed that the topmost Al electrode was damaged. As a result of electrode damage, the current was fluctuated I-V measurements, and a similar effect was also found in our previous paper [8,9]. In summary, under a lower current compliance, the conductive filaments of dendrites were reduced from the Cu ions. With increasing current compliance, the conductive filaments vaporized.

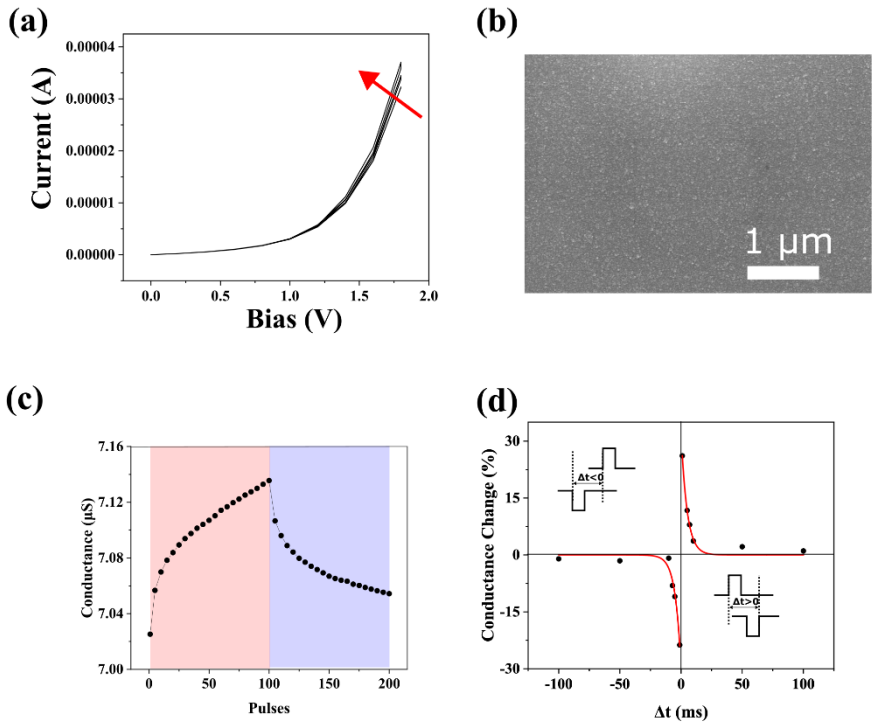

Figure 3 (a) Gradual SET processes of the Cu/Cu-doped TiO_2/Al memristive device from repeated positive sweeps ranging from 0 V to 1.8 V; (b) the surface morphology after I-V measurements from successive pulses presented in (a); (c) potentiation and depression of conductance modulated with positive (amplitude: 2.5 V, width: 100 ms)/negative spikes (amplitude: -1.8 V, width: 100 ms); (d) plot of the change in synaptic weight of the memristor as a function of time (Δt) and between pre- and postspikes (amplitude: 1.3 V, width: 20 ms).

The analog modulation of conductance in the memristive device was measured using identical consecutive sweeps from 0 V to 1.8 V with a step voltage of 0.01 V, and the results are shown in Figure 3. To observe a clear analog modulation of the memristive device, a positive DC sweep should not be higher than the SET threshold for digital data storage. Compared with the digital-type switching shown in Figure 2 (a), the maximum current in Figure 3(a) is considerably lower. After 3 consecutive sweeps, the memristive device was transferred for SEM imaging. There was no clear defect on the surface of the device, as shown in Figure 3 (b). The increase of conductance in Figure 3(a) is mainly due to the growth of conductive filaments. Figure 3(c) shows the conduction modulation using potentiation and depression with positive/negative spikes, which indicates that the conductance of the memristive device can be continuously regulated. This characteristic can be utilized for synaptic adjustment. Spike-Timing-Dependent Plasticity (STDP) was studied by applying programmed pre- and postspiking pulse pairs, as shown in the inset of Figure 3(d). The relative conduction change is defined as $\Delta W=(G_t-G_0)/G_0$, where G_t and G_0 are the conductance before and after the pre- and postspiking pairs, respectively. One can see that a considerably high synaptic change was present in the LTP (long-term potentiation) and LTD (long-term depression) processes, for which the STDP learning rule was realized. All these results were in agreement with the typical characteristics of biological synapses [8].

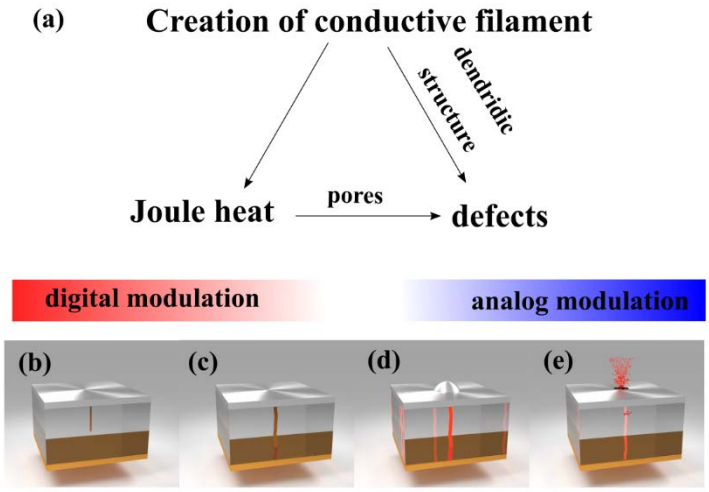

Figure 4 (a) Experimental mechanism; (b) the growth of filament in a memristive device operating for synaptic emulation; (c)-(e) creation, overheating and vaporization of conductive filaments in the memristive device.

In summary, the reproduction of defects was closely related to the Joule heat produced by the current flowing across a conductive filament, as shown in Figure 4 (a). The considerably low current shown in Figure 3 (a) indicates that the Joule heat is not prominent in the device for synapse emulations (analog modulation), in which the filament does not bridge the electrodes (Figure 4 (b)). Under a positive DC sweep with a low compliance current, the conductive filament grows within the body of the electrolyte layer; hence, the surface morphology of the memristive device does not change (Figure 4 (c)). Due to the increase in compliance current (0.1 A for digital modulation), conductive filaments started to grow on the top of the device (forming dendrites), became overheated (Figure 4 (d)) or even vaporized (forming pores, as shown in Figure 4 (e)).

Conclusion

In this paper, we reported a study of defects in a Cu/Cu-doped TiO_2/Al memristive device via current regulation, and the results suggested that Joule heating plays an important role in the creation of defects. For the I-V curve measured for digital application, defects were created in the SET process. Since the current required for synaptic emulation is much lower than that required for digital storage applications, there was no observable damage caused by Joule heating. These findings reveal a possible way to improve the performance of memristive devices in the future.

References

[1] B. Sueoka, K.Y. Cheong, F. Zhao, Study of synaptic properties of honey thin film for neuromorphic systems, Mater Lett 308 (2022) 131169. https://doi.org/10.1016/j.matlet.2021.131169.

[2] N. Ilyas, C. Li, J. Wang, X. Jiang, H. Fu, F. Liu, D. Gu, Y. Jiang, W. Li, A Modified SiO_2 -Based Memristor with Reliable Switching and Multifunctional Synaptic Behaviors, J Phys Chem Lett 13 (2022) 884–893. https://doi.org/10.1021/acs.jpclett.1c03912.

[3] X. Yan, J. Zhao, S. Liu, Z. Zhou, Q. Liu, J. Chen, X.Y. Liu, Memristor with Ag-Cluster-Doped TiO_2 Films as Artificial Synapse for Neuroinspired Computing, Adv Funct Mater 28 (2018). https://doi.org/10.1002/adfm.201705320.

[4] P. Bousoulas, J. Giannopoulos, K. Giannakopoulos, P. Dimitrakis, D. Tsoukalas, Memory programming of TiO_{2-x} films by Conductive Atomic Force Microscopy evidencing filamentary resistive switching, Appl Surf Sci 332 (2015) 55–61. https://doi.org/10.1016/j.apsusc.2015.01.133.

[5] I. Salaoru, A. Khiat, Q. Li, R. Berdan, T. Prodromakis, Pulse-induced resistive and capacitive switching in TiO_2 thin film devices, Appl Phys Lett 103 (2013). https://doi.org/10.1063/1.4840316.

[6] J. Joshua Yang, F. Miao, M.D. Pickett, D.A. Ohlberg, D.R. Stewart, C.N. Lau, R.S. Williams, The mechanism of electroforming of metal oxide memristive switches., Nanotechnology 20 (2009) 215201. https://doi.org/10.1088/0957-4484/21/33/339803.

[7] J. Kolar, J.M. Macak, K. Terabe, T. Wagner, Down-scaling of resistive switching to nanoscale using porous anodic alumina membranes, J Mater Chem C Mater 2 (2014) 349. https://doi.org/10.1039/c3tc31969e.

[8] B. Zhang, B. Gu, J. Petr, J. Rodriguez-Pereira, S. Slang, T. Wagner, Direct observation of conductive filaments from 3D views in memristive devices based on multilayered SiO_2: Formation, Dissolution, and vaporization, Appl Surf Sci 655 (2024) 159584. https://doi.org/10.1016/j.apsusc.2024.159584.

[9] S. Slang, B. Gu, B. Zhang, P. Janicek, J. Rodriguez-Pereira, T. Wagner, Direct visualization and 3D reconstruction of conductive filaments in a SiO_2 material-based memristive device, Physical Chemistry Chemical Physics 26 (2024) 10069–10077. https://doi.org/10.1039/D4CP00274A.

[10] B. Bharti, S. Kumar, H.-N. Lee, R. Kumar, Formation of oxygen vacancies and Ti^{3+} state in TiO_2 thin film and enhanced optical properties by air plasma treatment, Sci Rep 6 (2016) 32355. https://doi.org/10.1038/srep32355.

[11] L. Martin, H. Martinez, D. Poinot, B. Pecquenard, F. Le Cras, Comprehensive X-ray Photoelectron Spectroscopy Study of the Conversion Reaction Mechanism of CuO in Lithiated Thin Film Electrodes, The Journal of Physical Chemistry C 117 (2013) 4421–4430. https://doi.org/10.1021/jp3119633.

Author Contribution

Guangyu Wen and Bin Gu carried out the experiment. Bo Zhang wrote the manuscript with support from Tomas Wagner. Tomas Wagner supervised the project.

Funding

The author thanks for financial support from the grant of the Ministry of Education, Youth- and Sports of Czech Republic (grant LM2023037), the European Regional Development Fund Project, the project NANOMAT CZ.02.1.01/0.0/0.0/17_048/0007376 and the project of Faculty of Chemical Technology, University of Pardubice “Excellent teams”2023, the grant of Hebei Normal University (L2021B12) and the HeBei NSF (QN2023054)

Competing Interests

The authors declare that they have no conflict of interest.

Research Data Policy and Data Availability Statements

The data that support the findings of this study are available on request from the corresponding author, upon reasonable request.